THE BUCKLING OF CIRCULAR CYLINDRICAL SHELLS SUBJECT TO AXIAL IMPACT

By Anthony P. Coppa

Space Sciences Laboratory
Missile and Space Division
General Electric Company

SUMMARY

Early experimental results on the buckling of circular cylindrical shells subject to axial impact are described. A hypothesis for the mechanism of buckling which was based on these experiments is described. The results of further experiments which were designed to test predictions from the hypothesis and which appear to verify it in several aspects are then described.

INTRODUCTION

The work which this paper describes was undertaken several years ago in order to gain an understanding of the behavior of shell structures subject to axial impact. The motivation for this effort was the need to predict the forces which a shell structure, say of a missile or space vehicle, experiences when it suffers a collision with the ground. In many cases, payloads containing shock-sensitive components are mounted in such structures and must function during and/or after impact. In order to assure that the loading tolerances of these components are not exceeded, it is necessary to know in some detail what force pulses can be transmitted by the shell to these components throughout the phases of initial loading, buckling, and collapse.

The results of some early experiments are first discussed and a hypothesis for the mechanism of buckling due to axial impact presented. Later experiments which were designed to test predictions resulting from the hypothesis are then discussed and the results compared with the anticipated magnitudes and trends.

LIST OF SYMBOLS

$c = \sqrt{\frac{E}{\rho}}$	speed of compression waves
D	mean diameter of cylindrical shell
E	Young's Modulus
h	shell thickness
$K = \frac{\ell_y}{\ell_x}$	aspect ratio of buckles
ℓ	length of cylinder
ℓ_x, ℓ_y	axial and circumferential half wave lengths of buckles
ℓ_{cr}	critical length
ℓ_f	collapse length
M	impacting mass
m	mass of cylindrical shell
n	number of circumferential buckles
r	mean radius of cylindrical shell
$T = \frac{2\ell}{c}$	longitudinal period of compression wave
t	time
V, V_o	impact velocity
$\overline{V}_r$	velocity of contraction of buckle during postbuckling
$\alpha = \frac{m}{M}$	
δ	axial displacement of the cylinder end

δ_o, δ_i	maximum outer and inner lateral displacements of the polygon with respect to the initial circular cross section
ϵ	strain, unit axial shortening
ϵ_{cr}	critical strain
ϵ^*	initial strain
ν	Poisson's ratio
ρ	mass density of shell material
σ	stress
σ_{cr}	critical stress
σ^*	initial stress

EARLY RESULTS

Early experiments by the writer in which open ended thin cylindrical and conical shells were impacted longitudinaly showed that buckles of the familiar diamond form occur in an orderly fashion at the impacted end. The characteristic of these buckles is that they allow an almost total axial shortening of the shell surface with very little extensional strain. The materials used included paper, brass, steel, aluminum and the impact velocities ranged up to 35 ft/sec. In all cases, the buckle patterns were of essentially similar form for similar large ratios of the shell radius/thickness. Especially in the case of thin paper shells, the buckle patterns were notably orderly. Examples of such patterns obtained from experiments are shown in figure 1. The specimens, originally cylindrical shells of paper (r/h = 190, fig. 1a) and 2024 Aluminum alloy (r/h = 125, fig. 1b), are shown after having been expanded axially and, by virtue of this, flattened circumferentially. The axial and circumferential lengths are shown in the vertical and horizontal directions respectively and the impacted edge is at the top. The patterns consist of an array of folded triangular planes which in the fully collapsed configuration of the cylinder lie in the cross section plane. Two triangular planes which share a common base in the circumferential (horizontal) direction form the familiar diamond pattern. In figure 1a, the diamond patterns by and large are pointed at the four corners, at which adjacent patterns occur. The circumferential or inner folds are situated along a straight line. The diagonal or outer folds also lie along straight lines, these being inclined to the axial direction by the angle whose tangent is $K = \ell_y/\ell_x$, the aspect ratio of the individual buckles. In the fully collapsed form, that in which the shell is after the impact, the inner folds form essentially a regular polygon of n sides whose perimeter is equal to the initial circumference of the cylinder. In figure 1b the patterns are quite similar except that the horizontal points of adjacent diamonds do not touch precisely but rather, form the ends of short circumferential line segments. This latter property is characteristic of metal shells and becomes more pronounced for smaller r/h ratios. It is due primarily to the flexural rigidity of the shell wall which prevents sharp folding in the region of corners.

From the early experiments it was clearly evident that buckling occurs at the impacted end and progresses in discrete stages at the velocity of the impacting head. During the entire process there is a

region of collapsed material, folded in the manner described above, adjacent to the impacting head and an undisturbed region of the shell which extends from there to the other end. This observation was based on the appearance of specimens after impact and substantiated by high speed motion pictures. This phenomenon, that is, the localization of the buckling and collapse, occurs even when the end opposite the impacted end is merely placed on the base of the test apparatus with no other attachment or support.

Buckling and collapse progresses in the manner described over substantial percentages of the initial length, 90% not being uncommon for thin shells. An example of the sharp separation between the collapsed and undisturbed regions is given in figure 2 which shows a cylinder of 2024 Aluminum alloy before and after an impact at a velocity of about 21 ft/sec. having the following initial dimensions in inches: l = 27, D = 4.50, h = .004. The shell was dropped (together with a weight attached at the upper end) with no guidance of any sort against a flat base. Impact occurred, therefore at the bottom end.

The manner of testing was to impact the free edge of the shell vertically with a flat surface, either by dropping the shell (with a weight attached at the end opposite the impact) against a flat base or by dropping a flat plate on the edge of the stationary specimen. Initially there was no pressure differential across the shell wall, but as the shell collapsed, the pressure of the internal air increased, this being limited by an air vent. The internal pressure was sufficient to maintain roundness in the portion of the shell beyond the buckled region during the collapse process and hence contributed to the orderliness of the buckle deformations, especially for shells having high r/h ratios.

Due to the fact that the collapse configuration of the shell is a system of folded plane surfaces, it was asked whether this configuration could be described essentially by an inextensional deformation process. It was assumed therefore that the initial circumference of the cylinder has the same length as the perimeter of the polygon formed by the inner (horizontal) folds of the collapse pattern. The following procedure was used: Consider a circular cylinder of diameter D. Cross-section A which is initially circular becomes a regular polygon of n sides as it moves axially from A to C. (fig. 3a) The perimeter of the polygon equals the circumference. Now consider the circular cross-section which was in the undeformed cylinder at B. It becomes a polygon of n sides as it moves to C, this polygon being rotated about the cylinder

axis by the angle θ with respect to the former polygon. In fig. 3b the cross-section of the buckled cylinder at C is shown (for n = 5) in which both polygons are shown in their true relative positions when stations A and C are axially coincident. Cross-sections A and B which in the undeformed cylinder were circular are given by the polygons, $A_1A_2A_3A_4A_5A_1$ and $B_1B_2B_3B_4B_5B_1$ respectively. The cross-section at C has deformed into a polygon $C_1C_2C_3C_4C_5C_1$ which is coincident with $A_1A_2A_3A_4A_5A_1$. The originally cylindrical surface between stations A and C is reduced to 4n triangular plane surfaces: $A_1B_1A_2$, $A_2B_2A_3$, $A_3B_3A_4$, $A_4B_4A_5$, $A_5B_5A_1$, $B_1A_2B_2$, $B_2A_3B_3$, $B_3A_4B_4$, $B_4A_5B_5$, $B_5A_1B_1$, $B_1C_2B_2$, $B_2C_3B_3$, $B_3C_4B_4$, $B_4C_5B_5$, $B_5C_1B_1$, $C_1B_1C_2$, $C_2B_2C_3$, $C_3B_3C_4$, $C_4B_4C_5$, and $C_5B_5C_1$.

The dimensions of these triangles can be calculated easily. In figure 4 a plan view of a portion of the collapsed configuration is shown together with the arcs PQRST and $Q^1R^1S^1T^1U^1$ respectively of the original cross sections A and B (see fig. 3a). In the collapsed configuration the arc PQRST becomes the straight line segments B_1B_2 and B_2B_3 while the arc $Q^1R^1S^1T^1U^1$ becomes the segments A_2A_3 and A_3A_4. The segments form the congruent triangles $B_1A_2B_2$, $A_2B_2A_3$, $B_2A_3B_3$, and $A_3B_3A_4$ which, of course, lie in the cross section plane. The altitude of these triangles is determined as follows:

$$\ell_x = (r - \delta_i)\frac{(1 - \cos\theta)}{\cos}$$

From the assumption of inextensionality

$$\delta_i = r(1 - \theta \cot\theta)$$

Hence $\ell_x = r\frac{\pi}{n}\tan\frac{\pi}{2n}$ (1)

and since $\ell_y = r\frac{\pi}{n}$, the aspect ratio, $K = \frac{\ell_y}{\ell_x}$, of the collapse pattern is:

$$K = \frac{1}{\tan\frac{\pi}{2n}} \quad (2)$$

The quantities ℓ_x and ℓ_y can be shown to be the axial and circumferential half waves of the collapsed configuration. According to eqn. (2), as the number of circumferential waves in the collapse pattern increases, the triangular planes become more slender in the circumferential direction.

The pattern shown in fig. 1a has an average of five circumferential waves over the surface. The aspect ratio of the buckles is 3.0.

By comparison the aspect ratio derived from eqn. (2) (for n = 5) is 3.08.

The above relations, therefore, follow directly from the assumptions that the initial circumferential length of the cylinder is equal to the perimeter of the regular polygon of the collapsed configuration and that the axial length of the collapsed region is zero. They apply strictly to cylinders having zero wall thickness. Collapse patterns were constructed according to equation (2) and compared with patterns obtained from experiments. One such comparison may be seen in figure 5 which shows a partially expanded collapse pattern of seven circumferential waves obtained from a 2024 Aluminum cylinder of .004 in. wall thickness and an initial diameter of 4.50 in. The constructed pattern, also of n = 7 waves, agrees closely in overall appearance.

The orderliness of the experimentally derived collapse patterns stimulated the effort toward gaining an understanding of the process of buckling due to impact. An hypothesis, developed in an attempt to explain the mechanism of buckling, is given in reference 1. Because of the limited availability of this work, it is discussed in the following sections.

MECHANISM OF BUCKLING

The problem considered was the response of a thin circular cylindrical shell to an axially symmetric impact of a rigid mass against one end (see fig. 6). At the other end, the cylinder is supported longitudinally by a plane rigid surface. Both ends of the shell are assumed to be unrestrained against lateral displacement.

Loading due to Impact

The axial loading introduced into an elastic cylindrical shell by an axial impact prior to the initiation of instability may be taken, at least to a first approximation, from the solution of the longitudinal impact on an elastic bar. Donnell (Ref. 2) gives the solution for the stresses produced when a rigid mass of finite magnitude M strikes the end of an elastic bar which is supported rigidly at the other end. The total compression stress, $\sigma_n(t)$, at the impacted end is given by

$$\sigma_n(t) = \overrightarrow{\sigma_n(t)} + \overleftarrow{\sigma_{n-1}}\ (t-T),\quad nT < t < (n+1)\,T \qquad (3)$$

where the arrows indicate the sense of the wave motion, $\rightarrow$ being away and $\leftarrow$ toward the impacted end. $\vec{\sigma}_n(t)$ is given by

$$\vec{\sigma}_n(t) = \sigma^* \sum_{m=o}^{m=n} {}^{e}Z_m \sum_{h=o}^{h=m} \frac{m!\ (2Z_m)^h}{h!\ 2(m-h)} \qquad (4)$$

where $Z_m = 2\alpha\left(m - \frac{t}{T}\right)$ and $\alpha = \frac{\text{cylinder mass}}{\text{Impacting mass}}$.

$\vec{\sigma}_{n-1}(t-T)$ is obtained from $\vec{\sigma}_n(t)$ by taking n-1 and substituting (t-T) for t. According to this solution, the initial stress σ^* produced at the instant of impact travels at the sonic velocity as the front of a system of waves which increase in magnitude instantaneously by σ^* at each reflection from the ends.

When the mass M is infinite ($\alpha = 0$), its velocity is constant throughout the impact. Hence, the stress distribution in the bar is rectangular and its magnitude at any position (or time) is an integral multiple of the initial stress σ^*. This behavior is illustrated in Figure 7, which shows the variation of stress with time at each end of the bar. At the struck end, the stress is always an odd multiple of the initial stress: σ^*, $3\sigma^*$, $5\sigma^*$, etc., and at the other end, an even multiple: 0, $2\sigma^*$, $4\sigma^*$, etc., each value remaining for a time $\frac{2\ell}{c}$.

Impact by an Infinite Mass ($\alpha = 0$)

a) Initiation of Instability

At the instant of impact, a stress wave of magnitude $\sigma^* = \frac{V}{c}E$ propagates from the impacted end at a velocity $c = \sqrt{E/\rho}$. When the front of the wave has moved a distance $x = \ell_{cr}$ from the impacted end, instability will initiate during the first passage of the stress wave if σ^* is sufficiently large (see Figure 8). Instability occurs over this region because there is a geometrical configuration other than the cylindrical one which accommodates the axial displacement $\delta = \frac{V}{c}\ell_{cr}$ of the striking mass with a reduction in the axial strain. For regions of length $x < \ell_{cr}$, the cylindrical form is stable because other geometrical configurations which can contract by an amount δ cannot be generated by the imposed axial stress. Once instability has

started, the region $x = \ell_{cr}$ is not able to transmit the high level of axial stress which caused instability and, hence, the stresses transmitted to the remainder of the cylinder are insufficient to produce instability over that region. As a result, further axial displacement of the impacted end is accommodated by suitable displacements of the shell wall within the region $x = \ell_{cr}$, whereas the cylinder beyond the critical length remains relatively undisturbed.

In Figure 9, the variation of the total axial strain in the buckling part as anticipated by this mechanism is indicated. For the time from zero to $t = \frac{\ell_{cr}}{c}$, the strain remains at the value $\frac{V}{c}$. Instability occurring at $t = \frac{\ell_{cr}}{c}$ is accompanied by a rapid reduction in the axial strain in the unstable region. As the impacted end is continually displaced, the strain decreases due to the formation of other geometrical configurations in the buckling part, which have continually decreasing axial resistance. This is discussed under the section on post-buckling behavior.

Consider now an impact at a velocity which produces a stress wave of insufficient magnitude to cause instability in the first passage of the wave from $x = 0$ to ℓ. At $x = \ell$ and thereafter at every reflection from the rigid boundaries at each end, the stress abruptly increases by σ^* as was shown before in Figure 7.

In this manner, an initially low stress can increase to a value sufficient to cause instability. Since the stress increases by σ^* at each reflection, however, instability can occur at either end, depending on where the additional increment σ^* due to reflection makes the total stress sufficiently large to initiate instability over the region ℓ_{cr} adjacent to the particular end. If an even number ($N = 0, 2, 4, \ldots$) of reflections produces the critical stress σ_{cr}, instability must occur at the impacted end whereas for the case of an odd number ($N = 1, 3, 5, \ldots$) of reflections, instability must initiate at the end opposite the impacted end (see Figure 10).

Thus, the critical stress and time are given by the following relations:

$$\sigma_{cr} = (N + 1) \frac{V}{c} E \tag{5}$$

$$t_{cr} = \frac{\ell}{c} N + \frac{\ell_{cr}}{c} \tag{6}$$

Inextensional Buckling

A cylindrical shell subjected to axial loading buckles at a particular value of axial compression strain at which a geometrical configuration other than cylindrical provides the same axial shortening but with lower axial strain. Although such behavior can be called typical of all structures under axial compression loading, the cylindrical shell is singularly prominent in this respect. This is because its axial rigidity in the initial state is largely a result of its cylindrical form. However, even small lateral displacements from the cylindrical form cause large reductions in axial resistance. Yoshimura (Ref. 3) has shown that a cylindrical shell subjected to an end shortening can be developed into a surface which accommodates the axial shortening or displacement with a minimum of extensional strain. It is readily shown that if the trigonometric terms for the inextensional cross sections are retained instead of the approximations as used in reference 3, pp 6, 7, the unit end shortening is given exactly by

$$\epsilon = 1 - \sqrt{1 - K^2 \tan^2 \frac{\pi}{2n}} \qquad (7)$$

Eqn. (7) applies only to a cylindrical membrane ($h = 0$), but is useful for studying the buckling forms of actual shells having large r/h ratios.

According to eqn. (7), for a given value of ϵ, there exists an infinitude of surfaces each defined by a particular combination of K and n(2, 3, 4, . . .). Now suppose that a region of the shell a distance x from the end has an elastic axial strain of magnitude ϵ prior to buckling. Then if the surface assumes any one of the surfaces (defined by eqn. 7) corresponding to the given value of ϵ, the same amount of shortening will now be realized with no axial membrane strain. These surfaces consist of a system of plane triangles, the planes of which are inclined to the axis of the cylinder. The cross section of the inextensional surface is a regular polygon of n sides.

It is to be noted that when $\epsilon = 1$, which applies to total axial shortening, eqn (7) reduces to eqn (2) which was derived previously for the collapse configuration.

Because the edges of the cylinder were assumed to be free to move laterally, it was considered that the edge could suddenly change from a circle to a regular polygon when buckling was initiated.

Furthermore, construction of inextensional patterns showed that patterns consisting of one row of axial half waves were sufficient to accomodate any admissible value of ϵ and would have a lower density of fold line per unit axial length of surface. The density of fold line was taken as an indication of the bending strain energy that would be present in an actual shell. It was assumed, therefore, that the initial buckle pattern consists of a single row of axial half waves, that is, a single row of triangular planes.

L
3
1
0
9

A plot of some of these configurations is given in Figure 11, which shows curves of constant circumferential wave number. The unit axial shortening ϵ is plotted against the ratio ℓ_x/D of the axial half-wave length to the cylinder diameter. For a given ϵ, the configurations have the property that the smaller the axial half-wave length, the higher the number of circumferential waves. This property is illustrated in Figure 12, which shows several configurations corresponding to $\epsilon = .001$ in/in.

The ratio ℓ_x/D may be considered to be the initial dimensionless length of a region of the cylinder adjacent to one of its ends. If a given compressive strain, $\epsilon = \frac{V}{c}(N + 1)$ is imposed over the cylindrical region of a particular dimensionless length, there is one inextensional configuration which can provide an equal unit axial shortening with no axial compression strain over a region of the same initial length. This configuration is defined by a particular value of circumferential wave number n (2, 3, 4, . . .) and aspect ratio K.

Instability as defined herein is the change from the cylindrical form to an inextensional form having a particular n and K which provide, by inextensional deformation, the same unit axial shortening as the axial compression strain which existed in the cylindrical form.

In order to define a criterion for instability, reference is made to the previously stated relationship that for a given imposed unit axial shortening $\epsilon = \frac{V}{c}(N + 1)$, the shorter the axial wave length, the higher the number of circumferential waves. This suggests that cylindrical regions of small ℓ_x/D should require higher axial loading to become unstable than regions of larger ℓ_x/D. A further assertion is that the variation of axial resistance with ℓ_x/D should be increasingly stronger as ℓ_x/D approaches zero since the rate of rise of n and the fold-line density become increasingly greater as ℓ_x/D becomes very small. If ϵ_{cr} is the axial strain required to initiate instability, then instability will occur when the actual strain $\frac{V}{c}(N + 1)$ over a

region of length ℓ_x equals or exceeds the critical strain corresponding to that region. The criterion for instability is therefore

$$\frac{V}{c}(N+1) \geq \epsilon_{cr} \tag{8}$$

This criterion is illustrated in Figure 13 in which the critical strain is plotted against the ratio ℓ_x/D. Let a strain wave of magnitude ϵ proceed from the end of the cylinder designated by $\ell_x/D = 0$. As the wave travels along the cylinder, there is, at any instant, an inextensional configuration corresponding to the imposed value of ϵ. Since the critical value of axial strain of these configurations varies inversely with their axial length, the cylinder remains stable until the wave front has moved to the value of ℓ_x/D, at which the first configuration whose critical strain is equal to or less than the imposed strain exists. Then the cylindrical form becomes unstable over this length ℓ_x/D. This new configuration is the critical configuration.

Postbuckling Behavior

The postbuckling range is defined as the interval of buckling beginning with the critical configuration and ending with the collapse configuration. The collapse configuration corresponds to a unit axial shortening of unity and is defined by eqn. 2.

$$K = \frac{1}{\tan \frac{\pi}{2n_{cr}}}$$

An examination of the critical configuration shows that, at the vertices, an infinite curvature in the circumferential direction exists while all other locations along the cross section of the buckled surface have zero curvature (see Figure 14). This applies to the idealized inextensional surface in which the sides of the triangles are sharp folds formed by the intersections of adjacent plane triangles. In an actual cylinder, that is, one having a non-zero wall thickness, the initially buckled surface (see Figure 14) consists of alternating convex A and concave B surfaces (with respect to the initially circular cross section). The concave and convex surfaces correspond to the plane triangles of the ideal inextensional surface. The curvature in the circumferential direction of the convex surfaces is greater than that of the concave surface. Also, by considering the ideal inextensional

form, it may be seen that the displacement δ_o of the vertex from the initial cross section (outward in direction) is smaller than the displacement δ_i of the midpoint of the side of the polygon (inward). The ratio δ_i / δ_o of these displacements is given by

$$\frac{\delta_i}{\delta_o} = \frac{\sin \pi/n - \pi/n \cos \pi/n}{\pi/n - \sin \pi/n} \qquad (9)$$

and varies from a maximum value of 2.75 (n = 2) to a minimum value of 1 ($n \rightarrow \infty$). The generators of the cylinder, therefore, are more bent in the vicinity of the plane surfaces corresponding to the concave surfaces of the real shell than in the vicinity of the vertices. Because of these properties, the axial rigidity varies around the cross section of the critical surface in such a way that greater axial loading is concentrated in the region of the convex surfaces than near the concave surfaces. Thus, there is a preference to maintain the circumferential wave number of the critical configuration n_{cr}, throughout the postbuckling range.

The critical configuration must change in order to accommodate the further motion of the impacting mass of velocity V. Assuming that the shell maintains inextensional configurations having n_{cr} circumferential waves throughout the postbuckling range, it may be observed from Equation 7 that it is necessary for the aspect ratio K to increase continually since n_{cr} is fixed and ϵ depends on the displacement of the mass. The aspect ratio varies according to

$$K = \frac{\sqrt{2\epsilon - \epsilon^2}}{\tan \frac{\pi}{2n_{cr}}} \qquad (10)$$

Since $K = \frac{\ell_y}{x}$ and $\ell_y = \frac{\pi D}{2n_{cr}}$ remain constant, ℓ_x, the axial half-wave length of the buckling region, must decrease as ϵ increases. K can be related to the axial displacement of the mass by

$$K = \frac{2\frac{\delta}{\ell_f}}{1 + \left(\frac{\delta}{\ell_f}\right)^2} \cdot \frac{1}{\tan \frac{\pi}{2n_{cr}}} \qquad (11)$$

which is plotted in Figure 15. Referring to Figure 15, K rises rapidly and with decreasing rate as δ increases. The initial rate of increase of K is greater the higher the number of circumferential waves in the critical configuration. The reduction of ℓ_x is

produced by the axial displacement of the vertices of the inextensional configuration (initially located at a distance ℓ_{cr} from the end at which buckling takes place.) This behavior is illustrated in Figure 16. The configuration corresponding to $\epsilon = .001$ in/in may be considered as the critical configuration and those corresponding to $\epsilon = .01$, .1, and 1 representing various stages of postbuckling. These constructions result from Equation 10. It is interesting to note how the boundary between the buckling region and the remainder of the cylinder, a regular polygon of n_{cr} sides, approaches the end as greater axial shortening is imposed on the buckling region. The velocity $\overline{V}_r$ at which this boundary approaches the particular boundary adjacent to which buckling takes place is related to the impact velocity V by the relation

$$\frac{\overline{V}_r}{V} = \frac{1}{2}\left[1 + \left(\frac{1}{\frac{\delta}{\ell_f}}\right)^2\right], \quad \frac{\delta_{cr}}{\ell_f} \leq \frac{\delta}{\ell_f} \leq 1 \qquad (12)$$

This applies to buckling at either the impacted end, where the end of the cylinder is displaced at velocity V, or at the opposite end which is stationary. Equation 12 is plotted in Figure 17. This relative approach velocity, which is the velocity of axial contraction of the buckling surface, is much greater than V for small values of $\frac{\delta}{\ell_f}$ and becomes equal to V when $\frac{\delta}{\ell_f} = 1$. In terms of the unit axial shortening, the ratio $\frac{\overline{V}_r}{V}$ is given by

$$\frac{\overline{V}_r}{V} = \frac{1}{\epsilon} \qquad (11)$$

and, specifically for $\epsilon = \epsilon_{cr} = \frac{V}{c}(N + 1)$, the approach velocity is

$$\overline{V}_{r_{cr}} = \frac{c}{N + 1} \qquad (12)$$

d) Secondary Buckling

When the axial displacement δ of the striking mass is equal to the collapse length ℓ_f where

$$\ell_f = \frac{\pi D}{2n_{cr}} \tan \frac{\pi}{2n}$$

the axial length of the buckled region is zero (see Figure 16, $\epsilon = 1$). When the axial length equals the collapse length, the cylinder has

shortened by an amount ℓ_f and the previously moving vertices of the inextensional surface are coincident with the rigid boundary adjacent to which the instability took place. The approach velocity $\overline{V}_r$ at the instant when $\delta = \ell_f$ is V. Thus, independent of the end at which the buckling has taken place, a new impact of the longitudinally rigid boundary at velocity V against the new end of the cylinder takes place. This new end is, of course, a regular polygon having n_{cr} sides. The secondary impact, therefore, is against a cylinder whose impacted end has the form of a regular polygon in contrast to the initial impact against a circular end. The geometry of the surface adjacent to the end is the same as that described under the previous section, that is, the surface has varying axial rigidity around the cross section. Since the axial rigidity is higher near the vertices of the polygon than elsewhere, the major axial loading due to the new impact is introduced into the shell at the vertices. This latter set of vertices is displaced circumferentially from the corresponding vertices of the critical configuration by one-half circumferential wave length. Thus, there is a strong tendency for the same number of circumferential waves, and hence the overall geometry, as the previously developed buckled surface to form in all subsequent stages of buckling. Each stage of buckling contributes another row of triangular planes to the fully collapsed pattern formed in the preceding stages. Due to the aforementioned circumferential displacement of the vertices with each new stage of buckling, the overall collapse pattern has the appearance of regular parallelograms folded along their major diagonal. These diagonals form the sides of the regular polygon of the cross section plane. This is the familiar "diamond" configuration common to the buckling of thin-cylinder-like shells under axial compression.

Since each stage of secondary buckling is initiated by the collision of the impacting mass or the rigid base of the opposite end against the end of the stable part of the cylinder, collapse progresses along the cylinder at the velocity V.

Extensional Buckling

Buckling of the symmetrical or "ring" type is another mode of deformation other than axial strain which can accomodate the axial displacement. Indeed, from the viewpoint of the axial symmetry of geometry, loading, and constraint (since in actual practice, a truly free edge cannot be realized), it is to be asked whether this is not the mode of buckling which should occur initially over a wide

range of shell geometry and impact velocity. Even for the free edge condition, which implies no friction present between the edge of the shell and the impacting mass, there is an axially symmetric lateral displacement of the shell wall of the amount $\nu r \frac{V}{c}$ present at the front of the compression wave. This displacement can be a significant fraction of the shell wall, and not only introduces bending of the wall but also an axially symmetric circumferential compression strain in the region of the wave front. Both these factors can induce buckling. If lateral constraint of the shell wall is present as well, another axially bent and circumferentially strained (compression) region exists in the shell wall adjacent to the edge. The smaller the impact velocity, the smaller are all these effects, so it is to be expected that the symmetrical buckling mode is more likely (at least initially) for higher impact velocities.

e) Effect of Internal Pressure

It has long been apparent that the random nature of the initial imperfections of a cylindrical shell and the strong dependence of the axial rigidity on the cylindrical form produce large scatter and poor reproducibility in the experimental behavior of thin cylindrical shells subject to axial compression. Since the buckling behavior described herein is affected not only by the initial imperfections but also by their subsequent variation and magnification throughout the postbuckling range, a degree of disorder (although less than in static tests) is to be expected in experimental behavior. This is especially true for shells having large ratios of radius to thickness. In the experimentation, therefore, it has been necessary to allow a certain amount of internal pressure differential to be produced by the collapse of the internal volume of the buckling cylinder in order to reduce the effect of these random influences. This has been found to be of decreasing importance for thicker shells (i.e., those having relatively lower ratios of radius thickness).

EXPERIMENTAL TESTING OF PREDICTIONS

Predictions from the Theory

Several predictions follow from the mechanism described above. These are stated as follows:

1. The initial axial strain due to the impact rapidly rises to a value given by $\epsilon = \frac{V}{c}$.

2. If the velocity is sufficiently high this strain, after being sustained for a time, $t < \ell/c$, will rapidly decrease to a value which is small compared to the initial value, thereby indicating buckling. This buckling will occur at the impacted end.

3. If the velocity is smaller than the above value, but the momentum of the impacting sufficient, then the strain will rise in jumps due to reflections from the boundaries to a magnitude given by

$$\epsilon = \frac{V}{c}(N + 1)$$

until buckling, indicated by the first substantial reduction in strain, occurs. The time between discrete jumps in strain will be $t = \frac{2\ell_1}{c}$, for odd N and $t = \frac{2\ell_2}{c}$ for even N, where ℓ_2 and ℓ_1 are the distances from the strain measurement point to the impacted end and the opposite end respectively.

4. If the velocity is insufficient to cause buckling on the first passage of the compression wave, it is possible for buckling to occur at the end opposite the impacted end.

5. The critical buckling pattern, if it is of the inextensional form will be in the form of a row of triangular buckles whose aspect ratio is given approximately by eqn. (10). This is provided that the edge at which buckling occurs is free to move laterally.

6. During post buckling, the buckle size shortens axially from its initial form until the aspect ratio is as given by eqn. (2). The rate of shortening of the buckle pattern is initially much higher than the impact velocity and rapidly decreases as the collapse configuration is attained.

Experiments were conducted to test the hypothesis according to the above predictions.

Apparatus

The experimental apparatus used was the Precision Drop Tester,

located at the General Electric Company Space Sciences Laboratory (See Figure 18). This device consists of a hardened steel shaft 40 feet in length which is attached under tension between two vertically aligned points. A carriage situated concentrically with the shaft by means of two two ball bushings rides along the shaft. The impact head, a hardened and ground steel disc, 10 inches in diameter is mounted to the carriage. The carriage assembly (drop head) is hoisted to the drop height by means of an electric winch which is attached to the carriage by an electro-magnet. A hardened and ground steel base, 8 inches thick and 20 inches in diameter is mounted at the bottom end of the shaft and situated concentrically with it. The base is mounted on three adjustable screws for the the accurate positioning of the base in the horizontal plane. The carriage can also be adjusted with respect to the shaft so that the final alignment of the head with the impact end of the shell specimen can be accurately accomplished.

The drop head assembly contains ports for venting the air rapidly from the cylinder as it is collapsing. By means of this venting system, the buildup of internal pressure is prevented. The vent area can be decreased or completely closed according to specific requirements.

The specimen and its retainer are mounted on the base concentrically with the shaft. In order to do this the shaft must be raised clear of the base. This is accomplished by a manually operated winch.

Specimens

The specimens used in the experiments were cylindrical shells having the following dimensions: 5.70 in. inner diameter, 22.8 in. length and wall thicknesses of .004, .008, .016 and .019 inches. These correspond to a length to diameter ratio (ℓ/D) of 4 and diameter to thickness ratios of 1425, 712, 356 and 300. The materials used were the aiuminum alloys 2024 F, 2024 T3, and 5052 H-38 and 301 $\frac{1}{2}$ H stainless steel.

The specimens were fabricated from flat sheet by simply rolling

the sheet into a cylinder and making a longitudinal joint. Both rubber based and epoxy adhesives were used as bonding agents for the joints and both lap and double butt strap configurations were employed.

The specimens were simply cylindrical, containing no stiffeners. In most cases, the shells were mounted on a rigid circular base. The impacted end was initially free of support and was unconstrained from radial displacement during the impact except by friction forces at the impact interface.

Experimental Results

Initial Strain

Cylindrical shells of 2024 H-19 Aluminum alloy (D = 5.700 in., h = .008, l = 22.8 in.) were impacted at velocities of 11.5, 25, and 46 ft/sec. Strain gages were mounted to the cylinders in a back-to back manner (except where noted) at several circumferential locations and two axial stations, one at an inch behind the impacted end and the other at two inches from the opposite end. Tektronix oscilloscopes, triggered simultaneously by a common source, were used with Poloroid cameras to record the strain.

Typical strain records are reproduced in Figures 19, 20 and 21. These show the resultant compression strain near (one inch behind) the impacted end. The impact velocities are 46, 11.5, and 25 ft/sec. for Figures 19, 20 and 21 respectively. Figure 19, the short time record, has time and compression strain along the horizontal and positive verticle axes respectively. The time scale is 10 microseconds per unit grid spacing and the strain scale is .00196 in/in per unit spacing. A zero strain base is established (at the extreme left) by triggering the trace immediately prior to impact. It is seen that the strain rises within 10 microseconds to a peak strain of .00214 in/in and is sustained thereafter at an average level of .00194 in/in for 40 microseconds after initiation of the pulse (+85 μ sec. after impact) the strain has decreased to zero. The time required for the initial elastic stress wave to return to the forward gage position is 216 μ sec. It is apparent from this that buckling has been initiated during the first passage of the stress wave.

The axial compression strain produced by an impact at a velocity of 11.5 ft/sec. is shown in fig. 20. The pertinent scales are 50 μ sec. per grid spacing (horizontal axis) and .000783 in/in strain per unit

spacing (vertical axis). As before, the trace begins at the extreme left. The strain rises within 20 μ seconds to a value of .000802 in/in and after remaining at an average level of about .000622 in/in rises to a peak strain of approximately twice the initial peak. Thereafter, it decreases steadily and becomes equal to zero at 345 μ sec. after impact. It is interesting to note that the time at which the strain begins to rise to attain twice the initial value is slightly greater than 200 μ sec. after initiation of the signal. According to the loading mechanism in the theory a rapid rise in strain to twice the initial value is expected at 216 μ sec. when the compression wave reflected forward from the rear end arrives at the forward gage position.

The strain recorded for the test at a velocity of 25 ft/sec, shown in fig. 21 initially rises rapidly to a value of .00146 in/in. Thereafter the strain fluctuates about a similar mean value and then drops off rapidly. Only the initial portion of the trace, however, is offered as evidence since the measurement is due to a single axial gage. Bending strain components, therefore, may be present in the later portions of the trace.

Table 1

Impact Velocity ft/sec.	Measured Strain in/in	Predicted Strain in/in	Error %
46	.00214	.00274	-22%
25	.00146	.00149	-2%
11.5	.000802	.000684	+17%
	.000622*		-9%

*Average Strain during first passage of compression wave.

After buckling has been initiated, as indicated by the first reduction of axial strain, relatively small strains were measured during the entire long time trace. This was expected as previously discussed. In addition to the low total compression strain during this interval the measurements showed a considerable amount of bending of the shell wall. This is shown in Figures 22a and 22b which pertain to the test conducted at 11.5 ft/sec. These traces are from a pair of axial strain gages mounted back-to-back and wired to read separately. The time scale (horizontal axis) is 500 μ sec. per grid spacing and the strain scales (vertical) are

.000785 in/in (Fig. 22a) and .000783 in/in (Fig. 22b). After impact begins (at the extreme left) both traces show the compression strain pulse which is associated with the initiation of buckling. At about 400 μ sec. the traces run opposite each other, one reading tension and the other compression, thereby demonstrating axial bending of the wall. The bending strains run off the scale but the magnitude appears to be about .002 in/in or 2.5 times the maximum compression strain in the initial pulse. A composite plot of Figures 22a and 22b is shown in Figure 23, which reveals that the total compression strain present simultaneously with the bending strains is relatively low during the entire time trace.

The results described above appear to be in substantial agreement with predictions 1, 2, and 3 stated previously.

Buckling away from Impacted End

Buckling was obtained near the end opposite the impacted end with no buckling deformations present at the impacted end. This resulted from an impact at a velocity of 1.8 ft/sec. on a $\frac{1}{2}$ H 301 stainless steel cylinder (D = 2.50 in., h = .010 in., ℓ = 10 in.). This test was qualitative in nature and no measurements of strain were made. The buckle pattern that was present in the speciment after the test was very well formed and consisted of eight circumferential waves. The pattern went around the entire circumference and exhibited three rows of triangular buckles having an aspect ratio of about one. Other experiments of a more quantitative nature must be conducted to study the response of shells to impacts at such low velocity in more detail, but the test described seems to bear out prediction no. 4 to some degree.

Initial Buckling Configuration

High speed motion pictures were examined to study the initial buckling configuration. It was found that the initial deformation, which occurred almost immediately after impact, was rather axially symmetric over a very small axial length. Examination of the shell (r/h = 356) impacted at 46 ft/sec. (discussed previously) after the test showed that about .080 in. of the shell at the impacted end had bent through an angle of 90° into the cross section plane. This was followed by buckling in the triangular form. Another example in which the initial buckling mode was symmetrical is given in the sequence of photographs in fig. 24. The photographs show the behavior of a stainless steel cylinder (D = 5.70 in.,

h = .019 in., ℓ = 22.8 in.) impacted at 23 ft/sec. The pictures begin shortly after impact and show buckling initiating in the symmetrical form (plate 1). This buckle progresses through full collpase in one wave length. As full collapse is almost complete, the circular cross section at the rear end of the buckle changes into a polygon (plate 2). The probable reason for this is that a state of circumferential compression exists at the rear of the buckle due to radial inward displacement of the shell wall. As the inward radial displacement increases and with it the magnitude of circumferential compression, the circular section snaps into the shape of a polygon; thereby generating deformations of the quasi-inextensional form. Thereafter the triangular planes continue to rotate inward (plate 3) until they are almost in the cross section plane, at which time another row of triangular buckles are formed (plates 4, 5). The process continues as these latter buckles rotate into the cross section plane (plate 6).

It has been observed that formation of the initial symmetrical buckling is more pronounced for high velocities and lower friction coefficients at the impact interface.

Symmetrical deformation appears to be the initial form of response of a cylindrical shell to an axial impact, especially when the impacted edge is held circular and the velocity is high. When the shell is sufficiently thick, as, for example, fig. 24, the symmetrical buckling deformation serves as a transition between the circular constraint and a quasi-inextensional mode which dominates the further history of buckling and collapse. If the shell is quite thick, symmetrical buckling is the dominating mode for the entire history.

If the shell is thin, the symmetrical mode, although it is initiated quickly gives way to a quasi-inextensional mode that serves as a transition to the other (but lower) quasi-inextensional mode. Once this latter mode is produced, it dominates the further history of buckling and collapse.

From experiments on thin shells (r/h = 356 - 718), it appears that the observed patterns in this latter mode are similar to the initial patterns anticipated by the theory described herein. The patterns have the very low aspect ratios which the theory predicts for the given strain level and the observed number of circumferential waves. In addition these patterns exhibit the large and initially rapid shortening effect predicted the theory. This will be discussed later.

Due to the presence of friction at the impact interface, the experiments have imposed a constraint of possible lateral displacements of the shell wall, even though the shell is initially unsupported. The theory on the other hand considers an edge which is totally unrestrained in the lateral direction. Due to this difference, comparison of initial patterns between experiment and theory are not possible.

On the other hand, the fact that the patterns that dominate the longer history of post buckling are similar to the prediction of the theory and that these patterns occur when buckling has progressed sufficiently away from the edge, suggests that these patterns may be those which would be generated initially if the edge were unrestrained in the experiments.

Axial Shortening of Postbuckling Pattern

This phenomenon has been observed in high speed motion pictures. An example of this is given in fig. 25 which shows a cylindrical shell (D = 4.50 in., h = .004 in.) after its bottom end has impacted on a flat rigid surface at a velocity of about 18 ft/sec. The grid lines are one inch apart. In plate A, the triangular buckle which is very elongated in the axial direction is seen. In subsequent plates the buckle shortens axially by virtue of the downward motion (toward the impacted end) of the upper vertex. At the same time, the relatively small downward motion of the cylinder against the impacted surface is evident. Considerably superior photographic results have been obtained from a recent experiment with a thin conical shell having a semi-vertex angle of 5°. These photographs, which are presently not available in published form, demonstrate clearly the shortening phenomenon. The initial rate of shortening of the buckle pattern has been measured to be greater than 1000 ft/sec for an impact velocity of only 25 ft/sec.

For thicker shells, like that shown in fig. 24, the axial shortening of triangular patterns is much less than that described above. This is to be expected since the greater flexural rigidity interferes with the formation of highly elongated buckles in axial direction. It also is instrumental in maintaining substantial axial strength of the shell even in the late stages of postbuckling. As a result the buckling and collapse of thicker shells is accompanied by significant extensional strains.

ACKNOWLEDGEMENTS

The contributions to the experimental effort made by Mr. S. A. Cimorelli, Specialist, Experimental Stress Analysis, General Electric Company, are gratefully acknowledged.

The writer also acknowledges the support of the Aeronautical Systems Division, Air Force Systems Command, United States Air Force, which partially sponsored the investigations.

REFERENCES

1. Coppa, A. P., "On the Mechanism of Buckling of a Circular Cylindrical Shell Under Longitudinal Impact", General Electric Company TIS Rep. No. R60SD494, presented at Tenth International Congress of Applied Mechanics, September, 1960, published in Mechanics (USSR) - Periodical Selection of Translations of Foreign Articles, No. 6, 1961.

2. Donnell, L. H., "Longitudinal Wave Transmission and Impact", Transactions of the ASME, 1930.

3. Yoshimura, Y., "On the Mechanism of Buckling of a Circular Cylindrical Shell Under Axial Compression", NACA TM 1390, July, 1955.

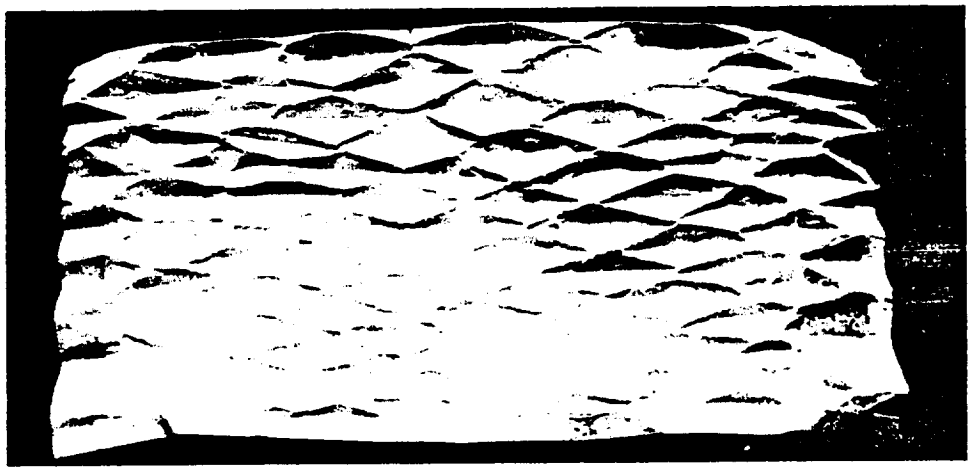

(a) Paper (r/h = 190).

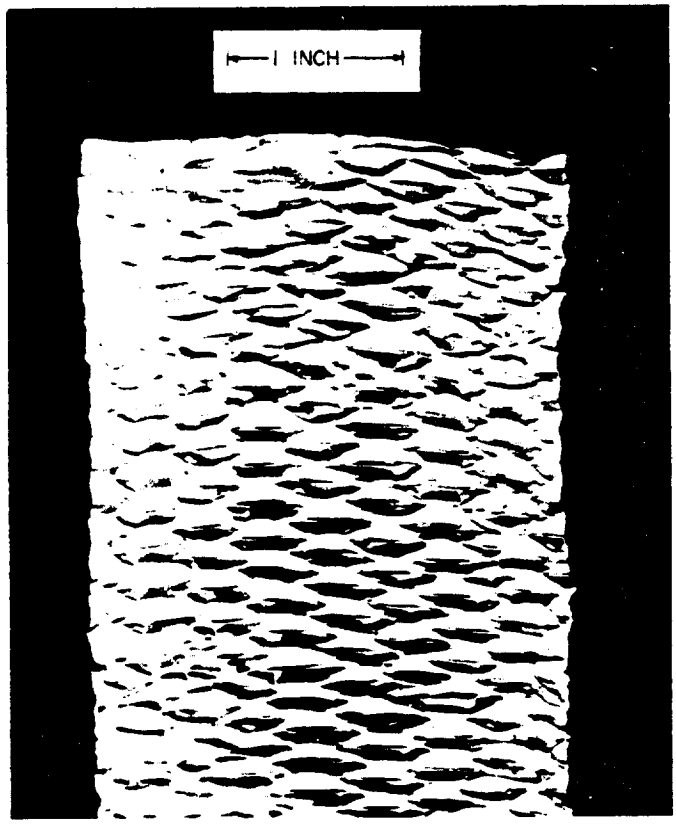

(b) Aluminum (r/h = 125).

Figure 1.- Collapse patterns in thin cylindrical shells.

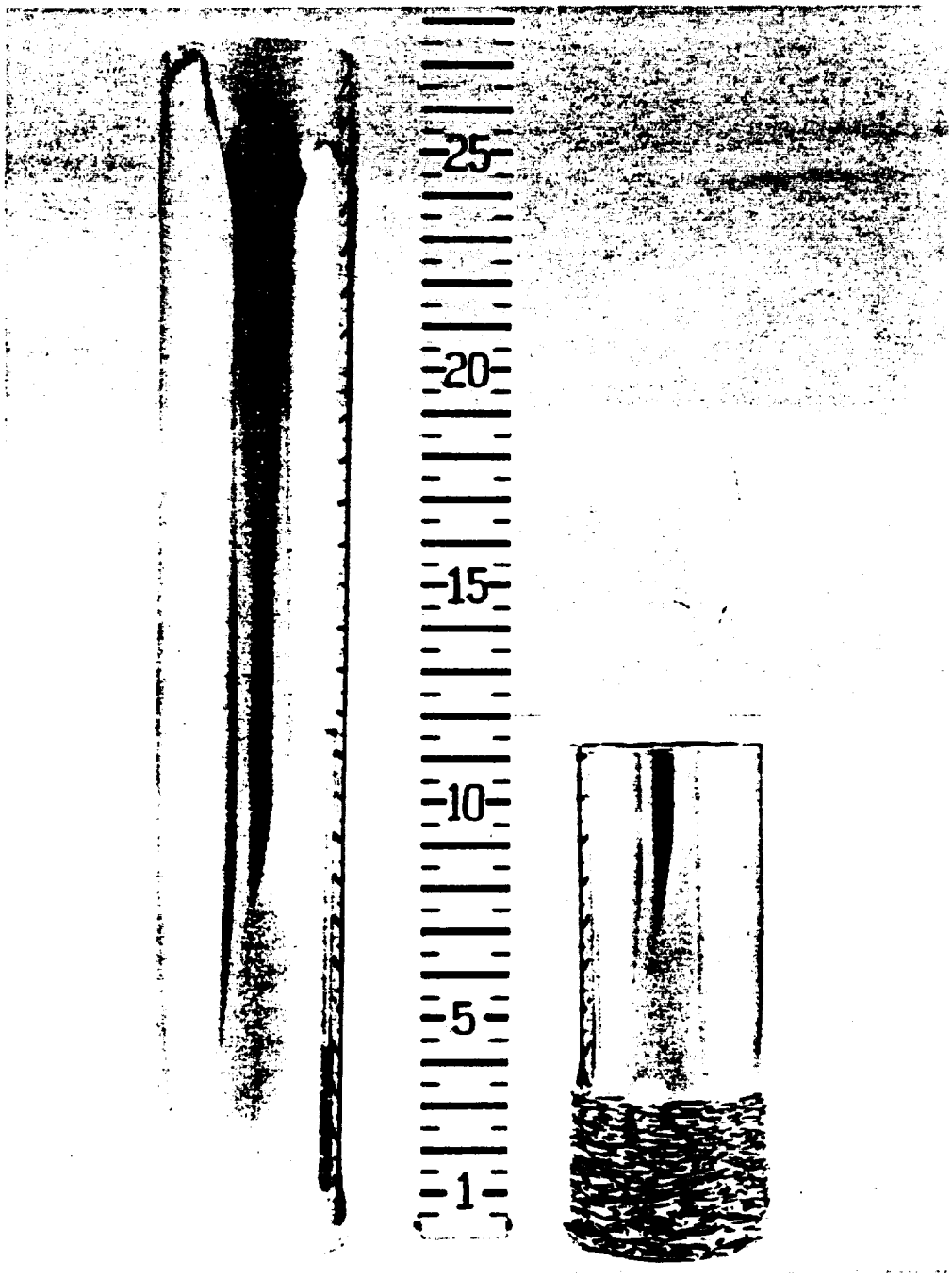

Figure 2.- Cylindrical shell before and after impact $(V_o = 21$ ft/sec$)$.

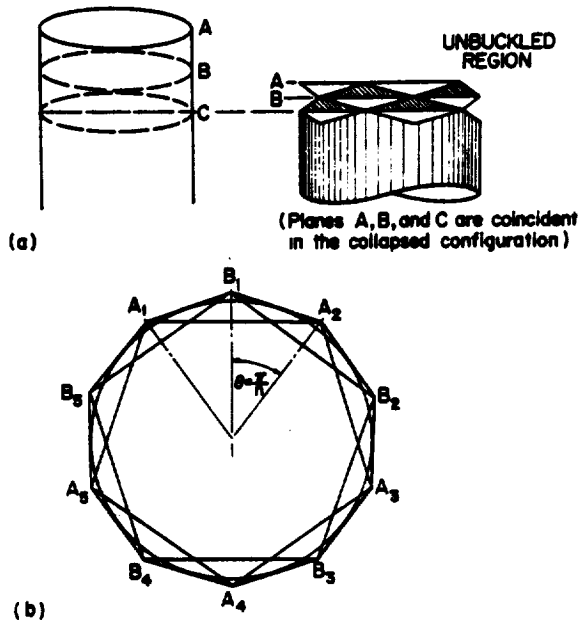

Figure 3.- Geometry of collapse - cross section.

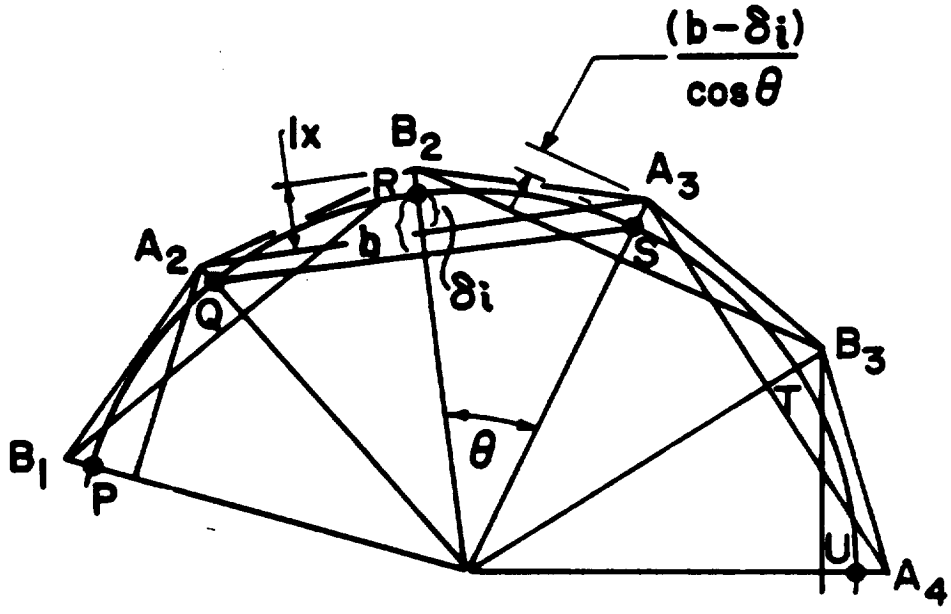

Figure 4.- Geometry of collapse - cross section.

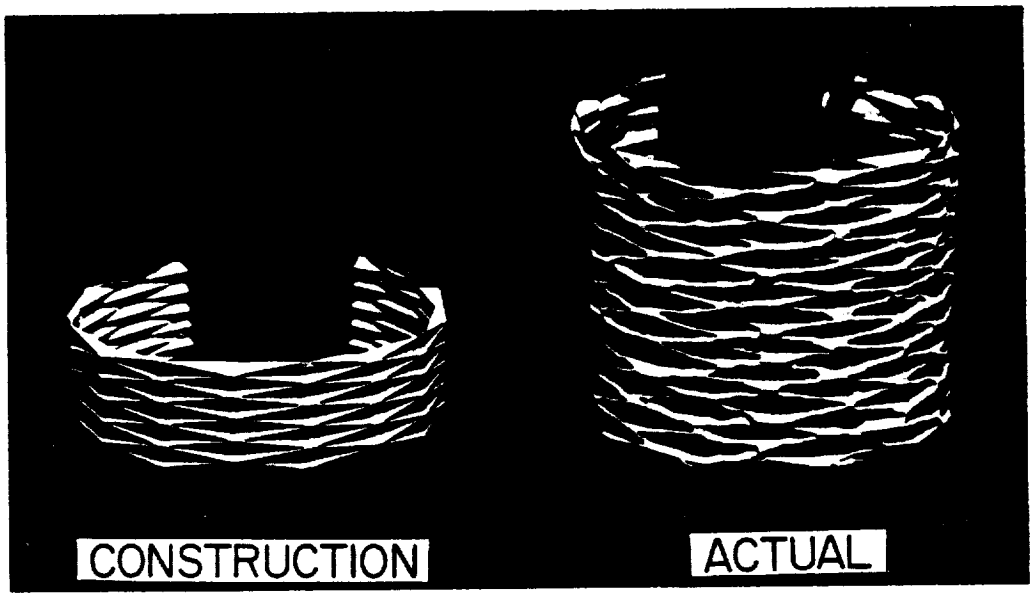

Figure 5.- Comparison of ideal inextensional and actual collapse patterns (n = 7).

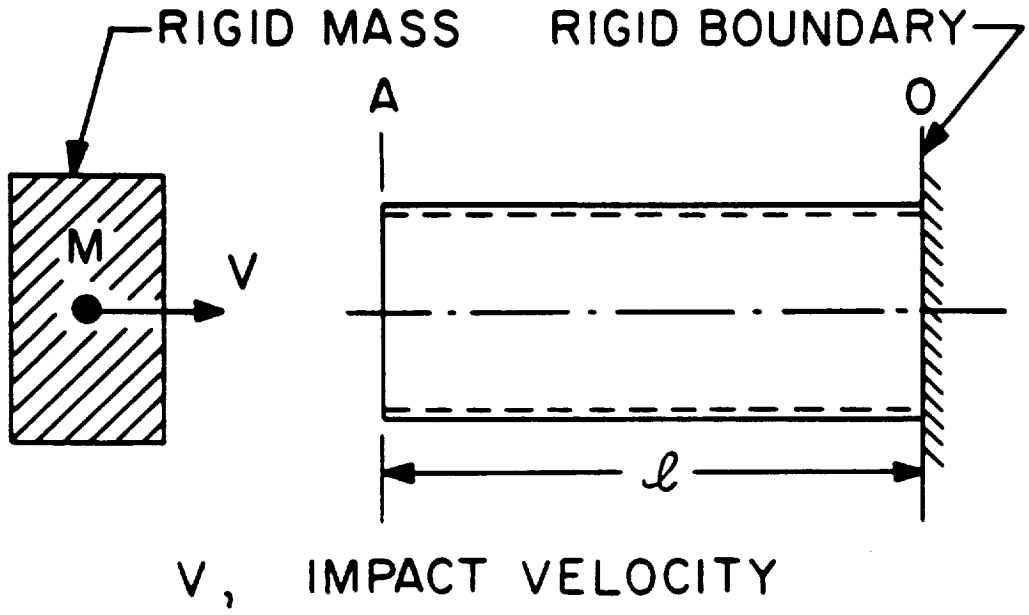

Figure 6.- Impact on a cylindrical shell.

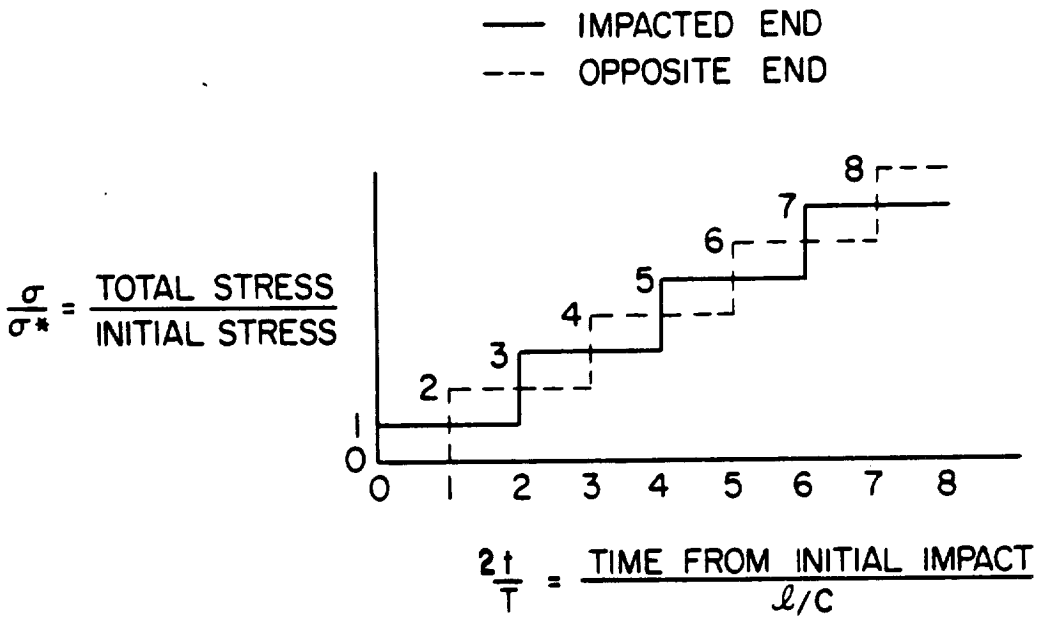

Figure 7.- Increase of stress due to reflections.

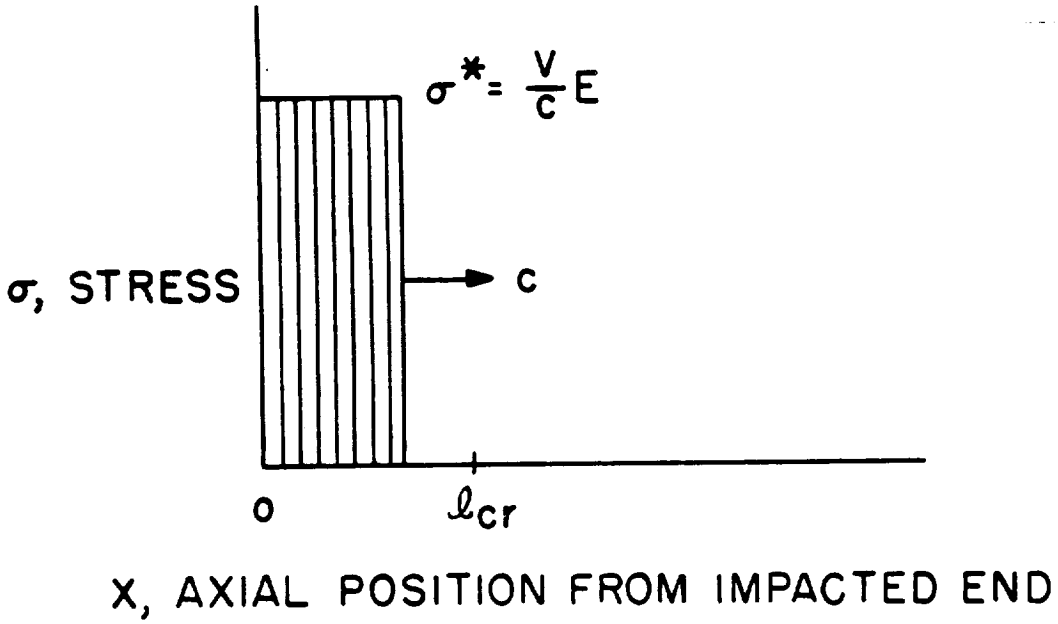

Figure 8.- Motion of the stress wave.

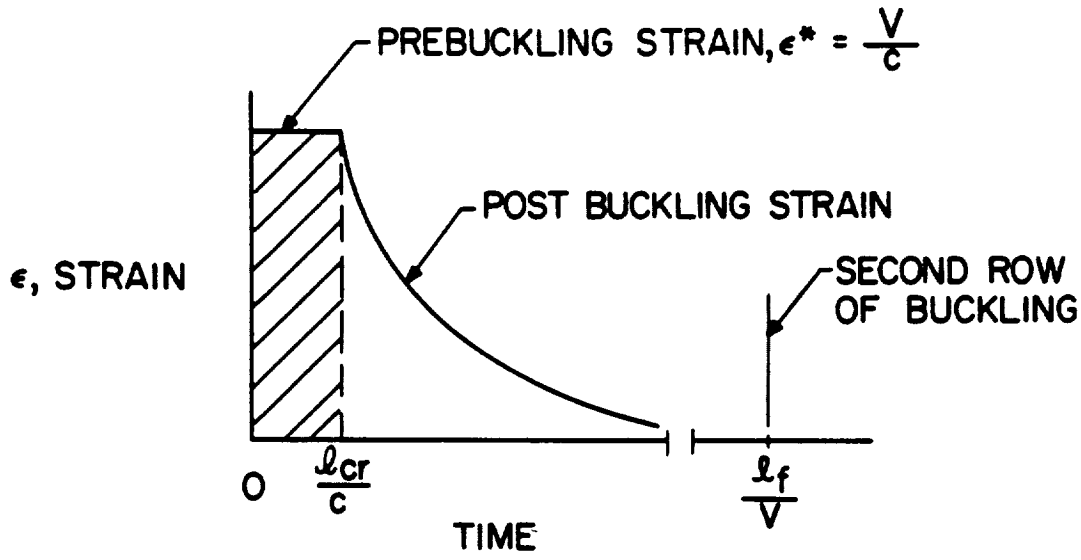

Figure 9.- Resultant axial strain in the buckling part.

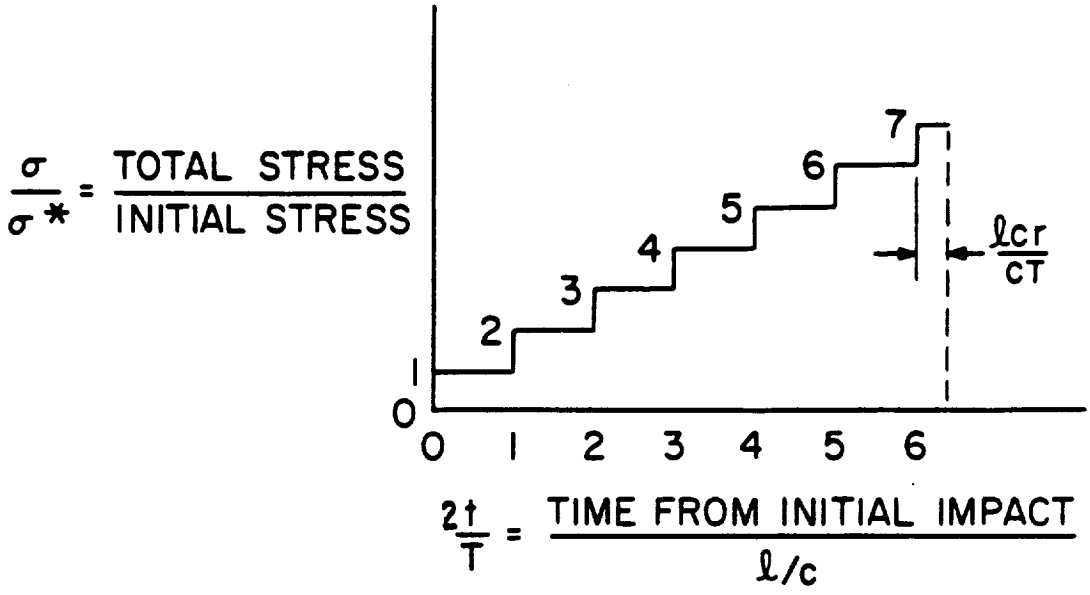

Figure 10.- Buckling resulting from reflections.

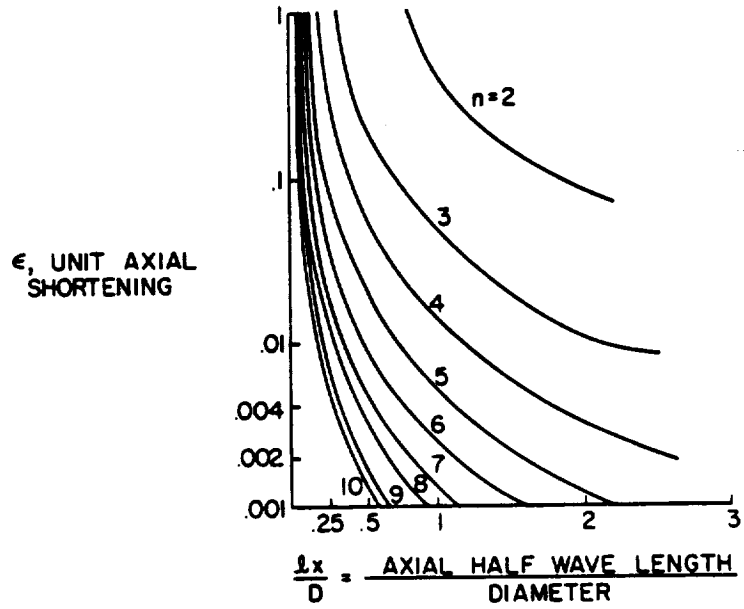

Figure 11.- Inextensional buckling configurations.

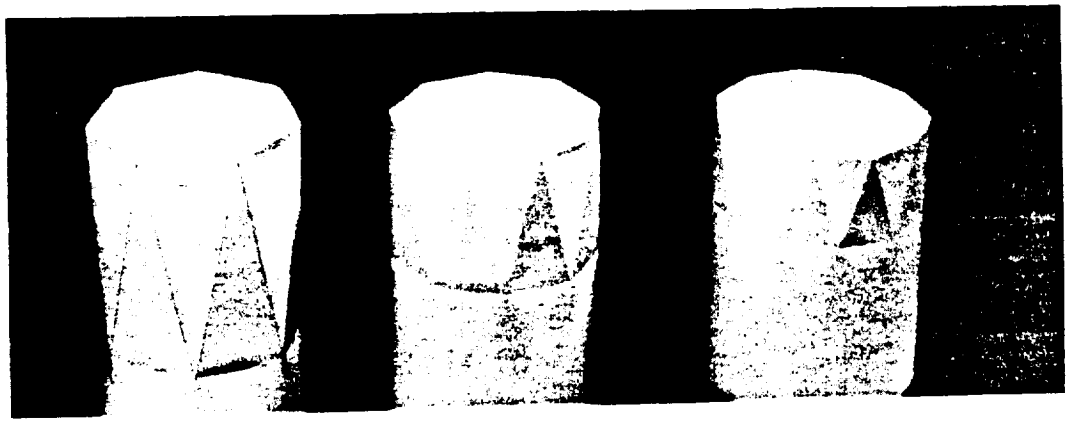

n = 7 ℓx = 5.02 in. n = 9 ℓx = 3.1 n = 11 ℓx = 2.06

Figure 12.- Inextensional buckle patterns $\left(\epsilon = \frac{1}{1000}\right)$.

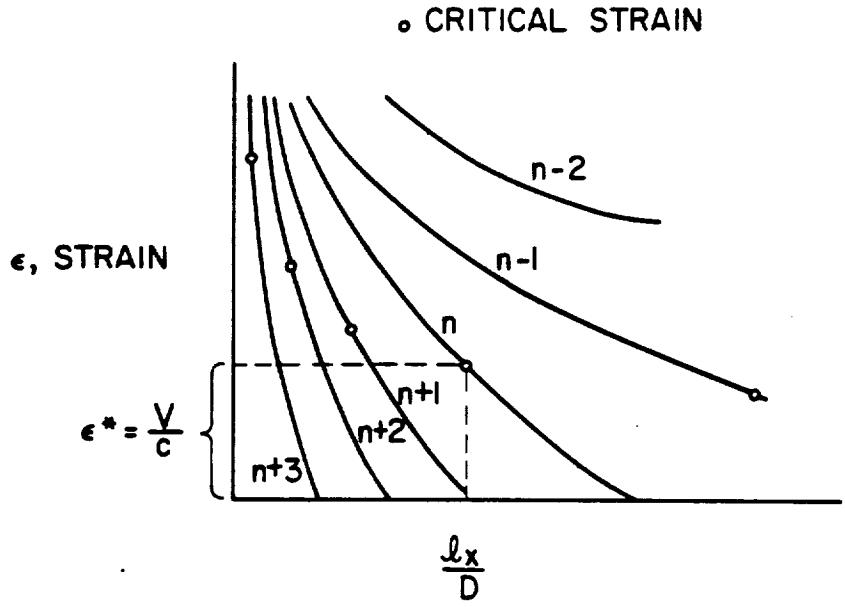

Figure 13.- Critical buckling configuration.

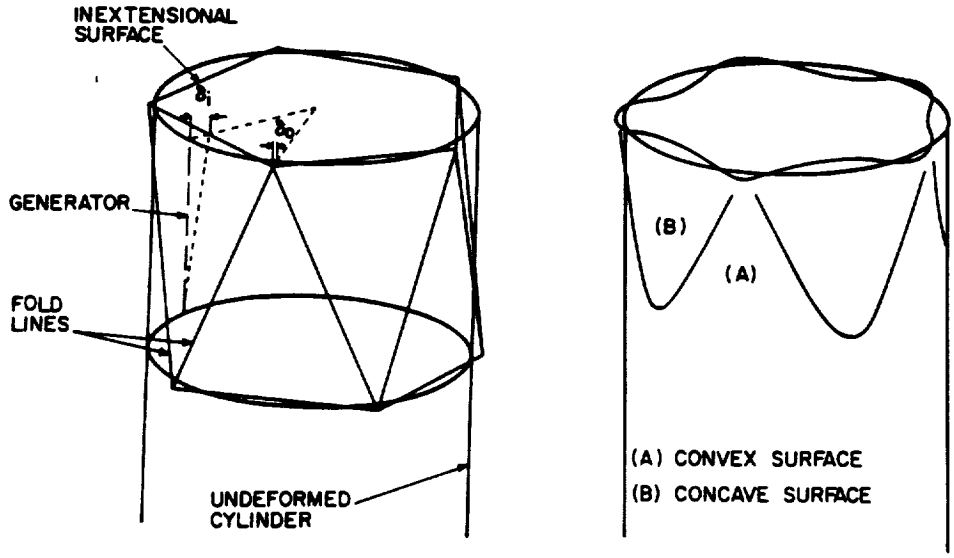

Figure 14.- Comparison of ideal and actual buckle surfaces.

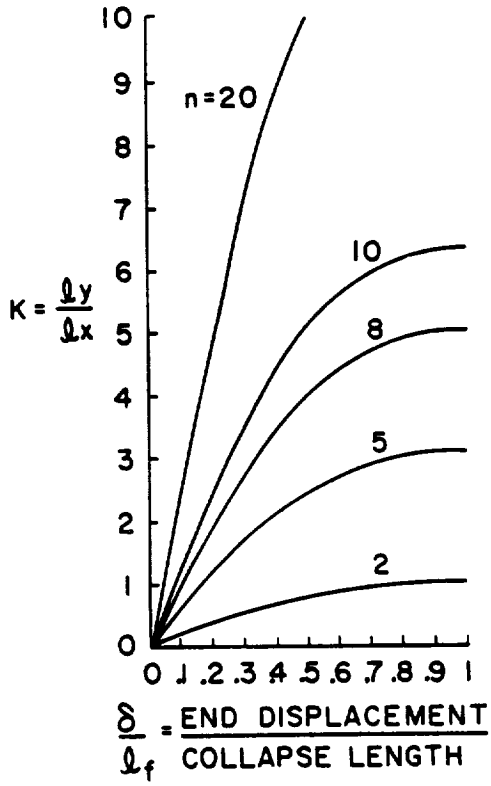

Figure 15.- Change of aspect ratio, K, during postbuckling.

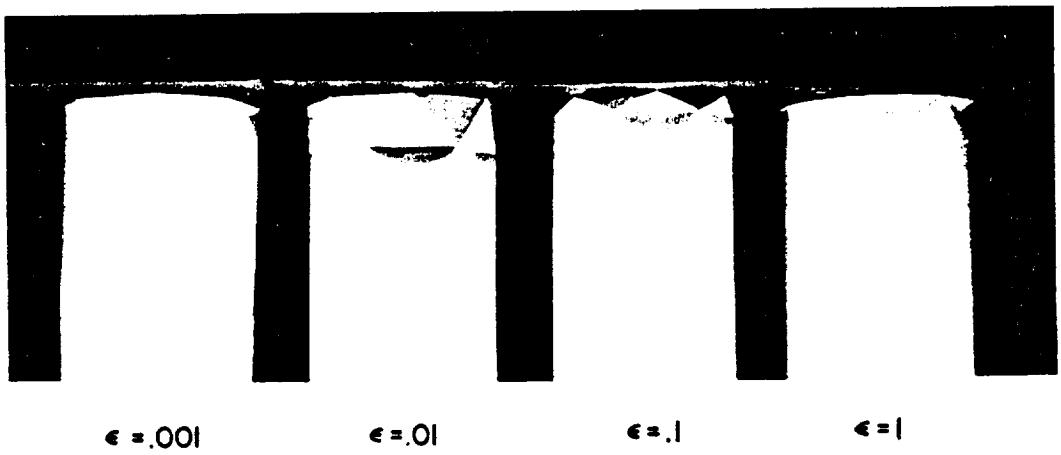

Figure 16.- Change of buckle pattern during postbuckling (n = 7).

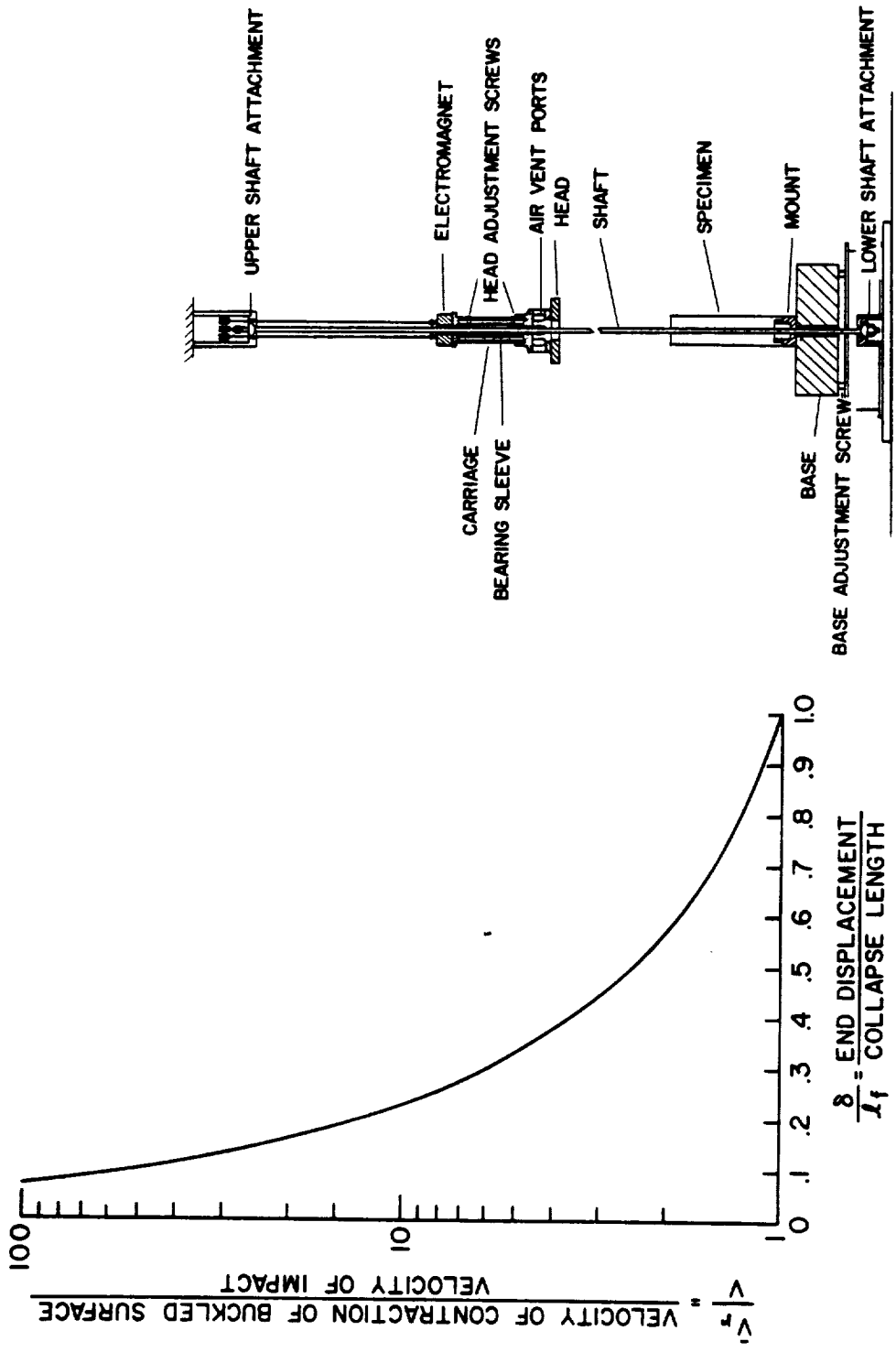

Figure 18.- Impact test apparatus.

Figure 17.- Axial shortening of the buckling region vs. end displacement.

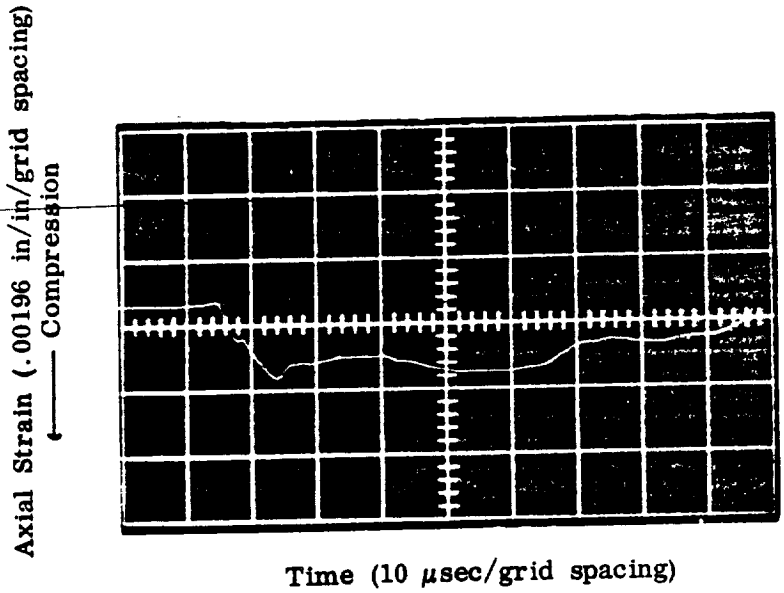

Figure 19.- Initial strain after impact $\left(V_o = 46 \text{ ft/sec}\right)$.

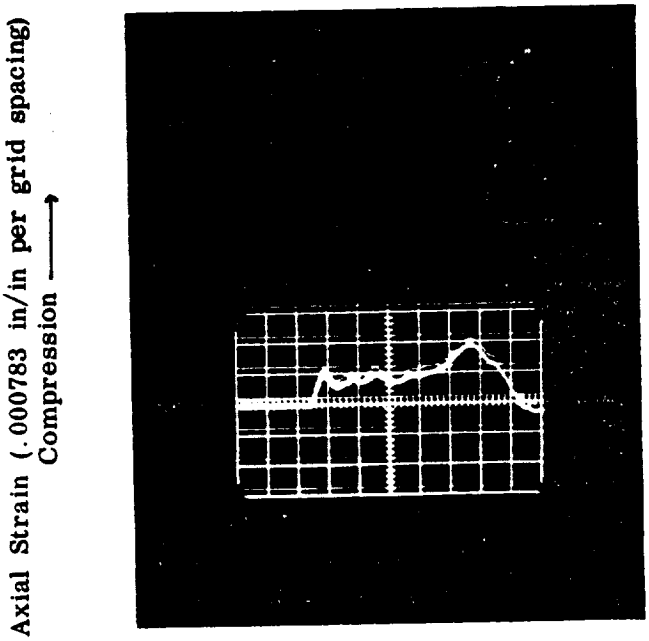

Figure 20.- Initial strain after impact $\left(V_o = 11.5 \text{ ft/sec}\right)$.

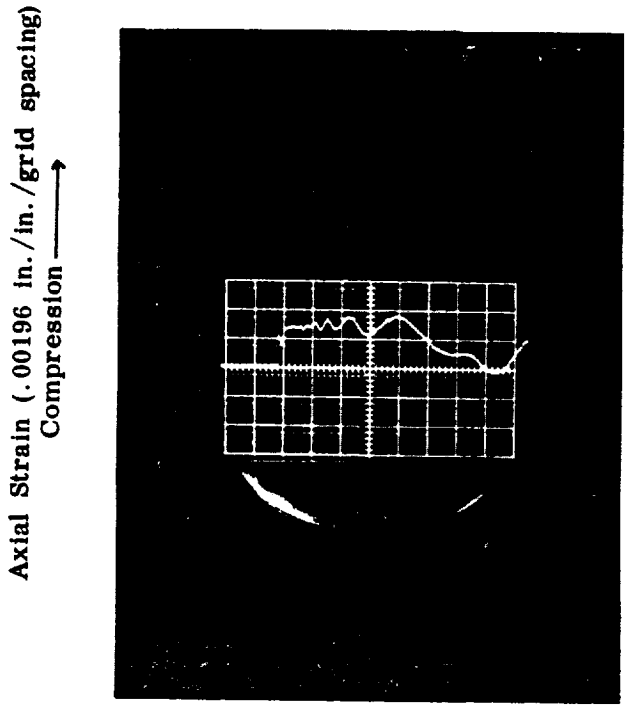

Figure 21.- Initial strain after impact $\left(V_o = 25 \text{ ft/sec}\right)$.

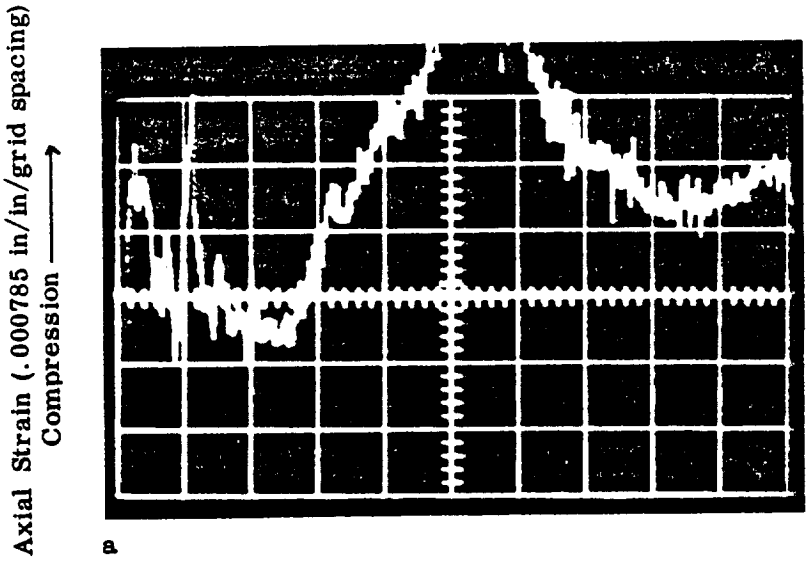

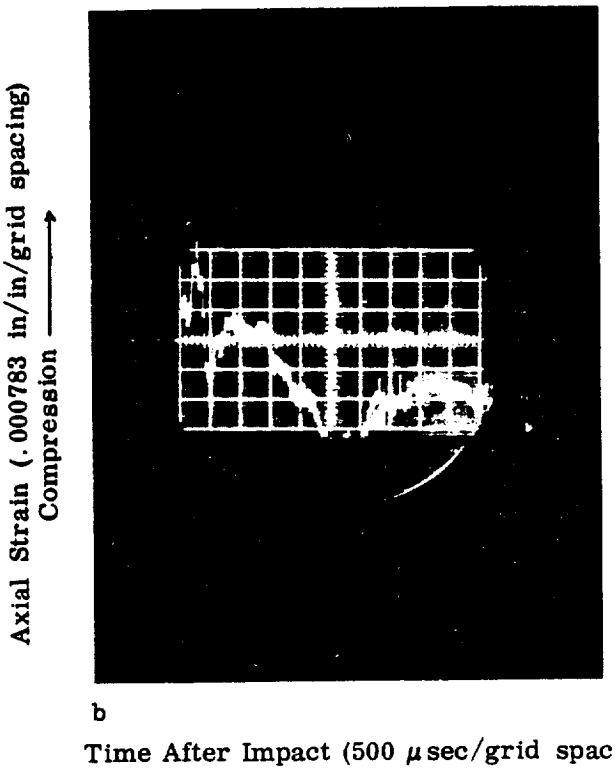

Figure 22.- Strain after impact $\left(V_o = 11.5 \text{ ft/sec}\right)$.

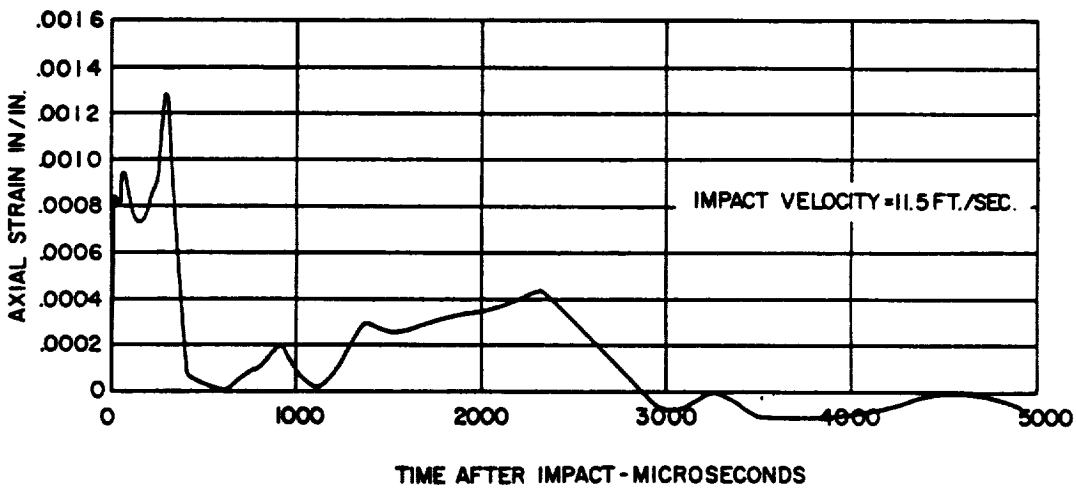

Figure 23.- Strain after impact $\left(V_o = 11.5 \text{ ft/sec}\right)$.

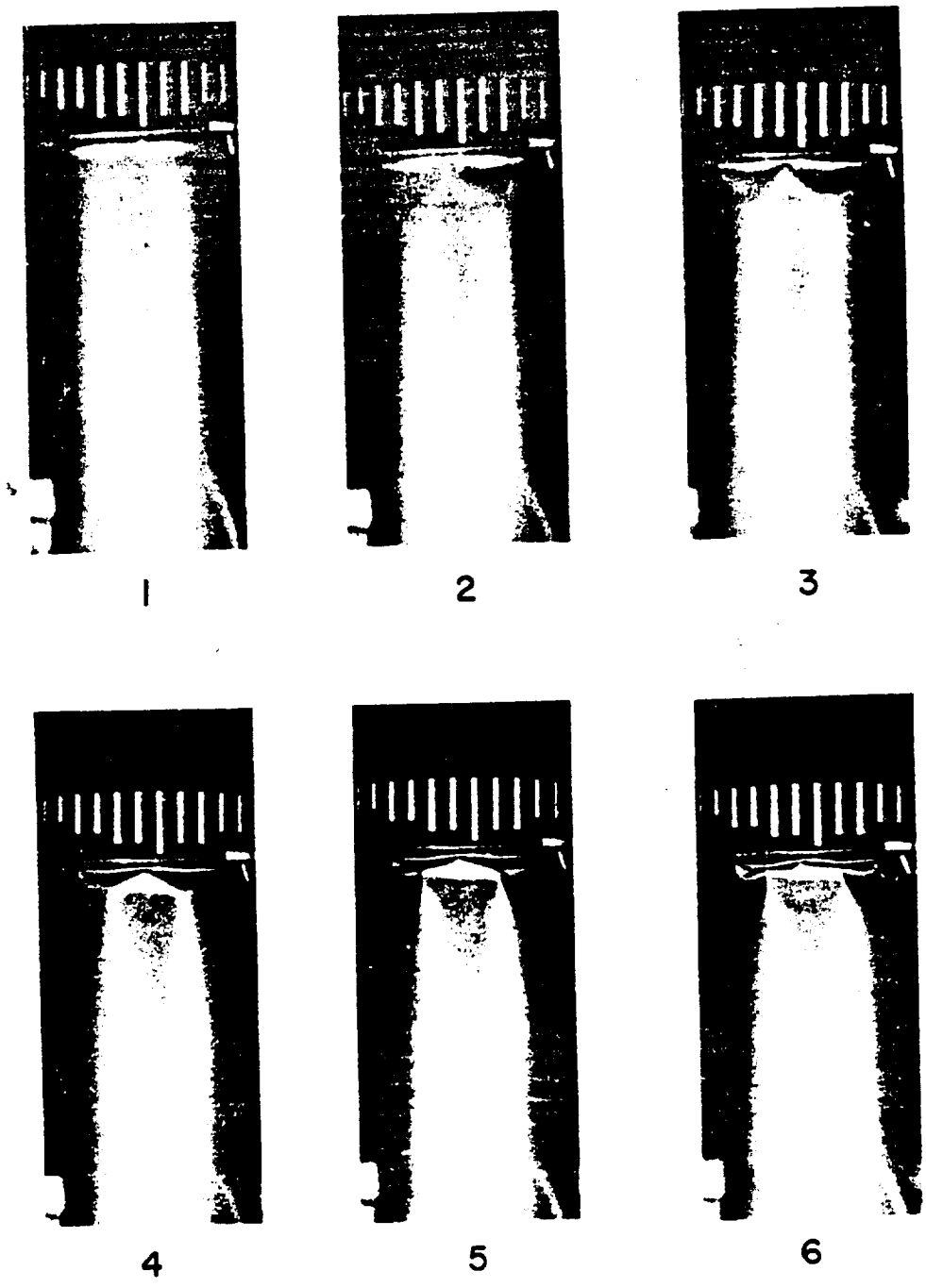

Figure 24.- Buckling sequence (V_o = 23 ft/sec).

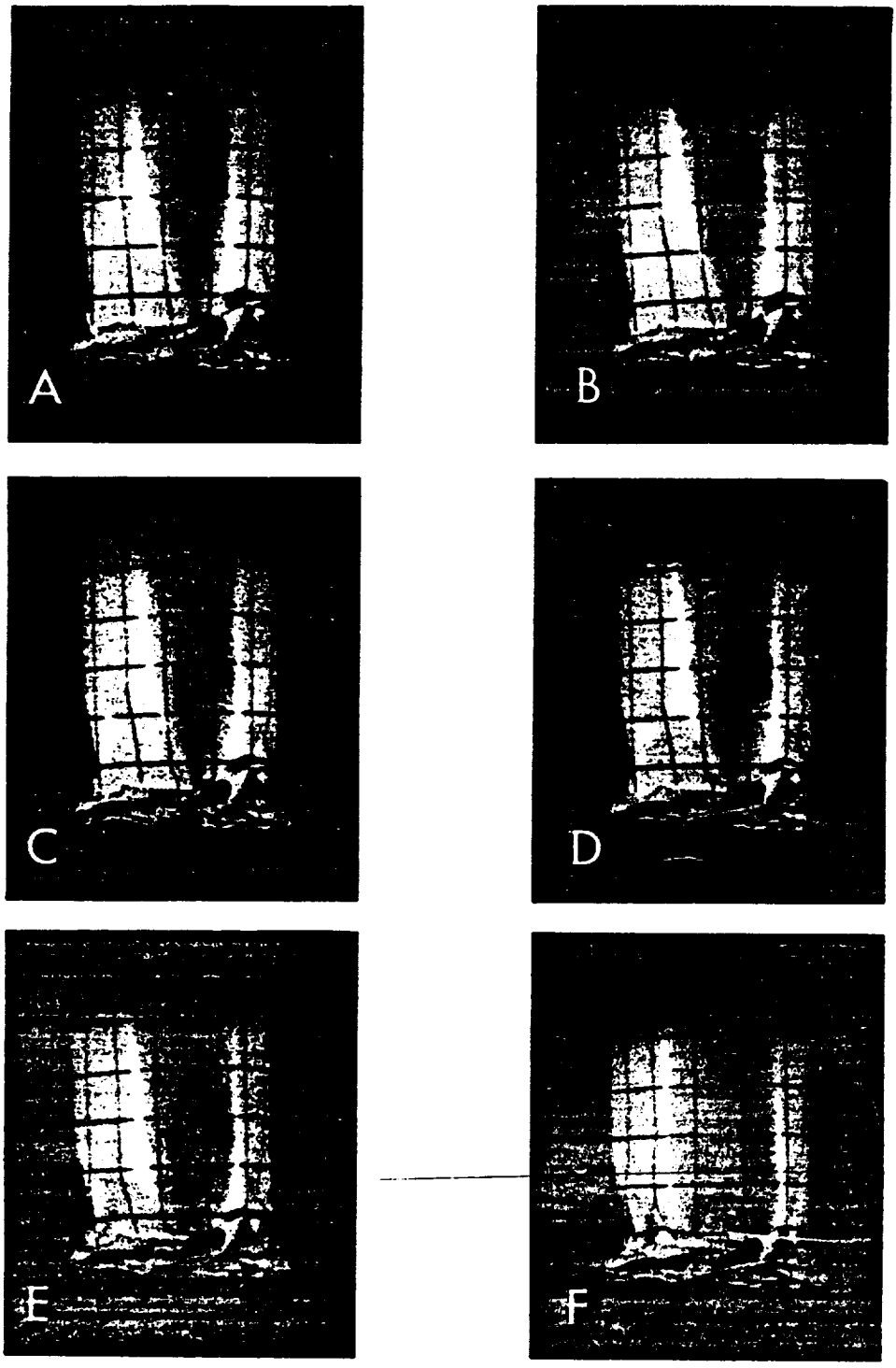

Figure 25.- Axial contraction of the buckled surface (from Fastax motion pictures).

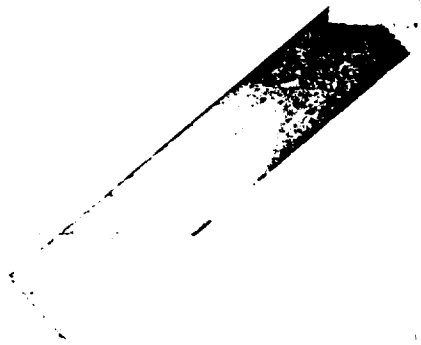

III CONICAL SHELLS